Open Access

OBM Neurobiology

LIDSEN Publishing Inc.

Original Research

Neuroprotective Effects and Cognitive Enhancement of Allomargaritarine in 5xFAD Alzheimer's Disease Mice Model

Yulia Aleksandrova [1], Alexey Semakov [1], Dmitry Tsypyshev [2], Kirill Chaprov [1], Sergey Klochkov [1], Margarita Neganova [1, *]

1. Institute of Physiologically Active Compounds at Federal Research Center of Problems of Chemical Physics and Medicinal Chemistry, Russian Academy of Sciences, 142432, Chernogolovka, Russia; E-Mails: aleksandrova@ipac.ac.ru; l_vok@list.ru; chapkir@gmail.com; klochkov@ipac.ac.ru; neganovam@ipac.ac.ru
2. Department of Medicinal Chemistry, Novosibirsk Institute of Organic Chemistry, Lavrentiev av. 9, Novosibirsk, 630090, Russia; E-Mail: sypyshev@nioch.nsc.ru

* **Correspondence:** Margarita Neganova; E-Mail: neganovam@ipac.ac.ru

Academic Editor: Talha Bin Emran

Special Issue: Natural Products and Their Bioactive Compounds for Treatment of Neurodegenerative Brain Disorder

OBM Neurobiology
2024, volume 8, issue 1
doi:10.21926/obm.neurobiol.2401207

Received: August 23, 2023
Accepted: December 18, 2023
Published: January 09, 2024

Abstract

Here, we report the results of an investigation of the neuroprotective effects of securinine with tryptamine conjugate-allomargaritarine (2b), previously selected as the leading compound among a wide range of natural derivatives. 2b was synthesized from securinine using various Lewis acids as catalysts. In addition to the antioxidant and cytoprotective properties previously shown for 2b, in this work, *in vitro* analysis of the biological activity of the compound demonstrated that this conjugate is also able to influence the primary pathogenetic mechanism of Alzheimer's disease - proteinopathy, modulating the homeostasis of β-amyloid peptide. In particular, it was found that 2b is an effective inhibitor of β-secretase 1 - an enzyme responsible for initiating the generation of pathological forms of β-amyloid peptide, as well as directly preventing the pathological aggregation of $A\beta_{1-42}$. As a compound

with a promising biological activity profile found *in vitro*, 2b has also demonstrated excellent neuroprotective effects on the *in vivo* 5xFAD Alzheimer's disease transgenic mice model. Thus, 2b effectively restored cognitive dysfunction: short-term and long-term episodic and spatial memory, which in the *post-mortem* studies was also accompanied by a decrease in the number of amyloid deposits and the intensity of oxidative stress in brain samples. These results provide an opportunity to draw a line under years of research on the neuroprotective potential of 2b as a viable therapy for Alzheimer's disease.

Keywords
5xFAD transgenic mice; β-amyloid; BACE1; antioxidant; allomargaritarine; alkaloid securinine; stereospecific synthesis; docking

1. Introduction

Alzheimer's disease (AD) is the most common age-related neurodegenerative disease [1]. To date, only symptomatic treatment can improve the patient's quality of life for a short period. The current therapeutic strategy for AD aims to create single-target drugs that regulate either β-amyloid (Aβ) aggregation, tau phosphorylation, or selectively inhibit glutamate receptors [2, 3]. The successful anti-AD agents should also target the leading abnormal biochemical cascades during neurodegeneration, including excessive activation of oxidative stress (production of reactive oxygen species (ROS)), mitochondrial dysfunction, neuroinflammation, and others [4, 5]. Therefore, the multifactorial mechanism of AD etiology and pathogenesis requires searching for versatile molecules with a high therapeutic index. It is preferable to design and synthesize as an agent that can simultaneously interact with several pathological components, thereby comprehensively preventing the development and/or relieving AD symptoms.

The prospect of searching for desirable compounds among substances of natural origin is supported by their multipurpose biological activity, availability, and capacity for modifications. Historically, most new drugs have been developed from natural products or their secondary metabolites and derivatives.

From the point of view of therapeutic approaches related to AD, among various groups of natural compounds, alkaloids of the securinine type are one of the most pharmacologically interesting groups of natural compounds. This type of alkaloid belongs to the indolizidine alkaloid family, in which the indolizidine moiety is incorporated into an unusual tricyclic structure.

Securinine, the best-known member of this group, has been used in the past as a nervous system stimulant and is now used in traditional medicine in several countries to treat various pathological conditions [6-8].

Securinine (1) has unique structural characteristics. Its rigid molecule contains four rings, starting with 6-aza-bicyclo[3.2.1]octane essential structure, to which an α,β-unsaturated-γ-lactone and a piperidine ring are annelated. Among all minor securinine-type alkaloids, the most interesting is margaritarine, originally isolated from the endemic tropical tree Margaritaria indica Dalz [9]. According to its structure, it can be represented as a derivative of allosecurinin (2-epi-securinine) [9].

Margaritarine contains an N-tryptamine moiety as a peripheral substituent. Replacement of the multiple bonds with sp^3-hybridized carbon atoms and the presence of an additional asymmetric center lead to a specific conformational mobility of the margaritarine molecule, which increases the possibility of its interaction with receptor active centers [10]. It could have remained an object of little interest due to its inaccessibility if it had not been shown [10] that its closest analog, allomargaritarin (2b), can be obtained directly synthetically from the more accessible securinine alkaloid. Structurally, 2b can be represented as a conjugate of securinine (1) and tryptamine, and given the tryptamine attachment site, it can be assumed that it can be obtained by the aza-Michael addition reaction from securinine (1).

Our previous biological activity data indicated that 2b has high antioxidant and mitoprotective activities [11]. The agent effectively defended the rat brain cortex cells from Aβ-induced neurotoxicity [11]. In a series of *in vivo* experiments, it was found that the administration of 1 to mice at a dose of 20 mg/kg led to the development of severe convulsions. In contrast, no convulsions were observed when 2b was administered at the same dose [12]. In other animal models of epilepsy, multiple administration of 2b decreased the latent period of seizures, suggesting that this substance has anticonvulsant properties [12, 13]. So, the neuroprotective properties of 2b indicated its potential applicability as an anti-AD treatment, which may deliver more effective protection [14].

Therefore, in this study, we have improved the method of obtaining 2b and set out to identify a new probable pharmacological potential of 2b as a promising therapeutic agent against Alzheimer's disease using the 5xFAD transgenic animal model. Additionally, to establish the possible mechanisms of the neuroprotective action of 2b against proteinopathy and oxidative stress, *in vitro* and *post-mortem* studies were conducted.

2. Materials and Methods

2.1 Chemistry

Synthesis of (2R-,7S-,9S-,15R-)-15-(2-indol-3-yl-ethylamino)-14,15-dihydro-securinan-11-one (2a, A-isomer, 2,15-di-*epi*-margaritarine) and (2R-,7S-,9S-,15S-)-15-(2-indol-3-yl-ethylamino)-14,15-dihydro-securinan-11-one (2b, B-isomer, allomargaritarine, 2-*epi*-margaritarine).

2.1.1 Method A. Reaction Catalyzed by Ytterbium Triflate

500 mg of securinine (2.304 mmol) were dissolved in 20 ml of methanol, 406 mg of tryptamine (1.1×, 2.534 mmol, Sigma-Aldrich), 143 mg (0.1×, 0.23 mmol) of ytterbium triflate were added, sealed and left at room temperature. The reaction proceeds very slowly. After two days, only traces of products are detected by TLC. After 6 days, spots of new substances in significant amounts appeared on TLC. The reaction mass was evaporated under reduced pressure. Without further separation, the residue was applied to a silica gel column eluted with a mixture of $CHCl_3$ + 1% NEt_3 with an increasing gradient of isopropanol. TLC controlled the composition of the fractions in the system $CHCl_3$:IPA:NEt_3 = 20:2:0.15 on silica gel plates (Merck KGaA), detection with phosphomolybdic acid, and heating with a heat gun. Moreover, in such a system, Rf (securinine, 1) = 0.77, Rf (2a) = 0.31-0.41, Rf (2b) = 0.23, and Rf (tryptamine) ≈ 0, all dark spots on a yellow background. The mixed fractions were rechromatographed. The target product, allomargaritarine

(isomer 2b), was isolated in pure form in 174 mg (0.46 mmol, 20%), an amorphous foam, after drying in an oil pump vacuum from the ether. It darkens after a few months of storage.

2.1.2 Method B. Long Reaction Catalyzed by Ytterbium Triflate

Repeating the previous reaction, but when incubated for 14 days, led to similar results. After purification, isomer 2b was isolated on column chromatography in 177 mg (0.47 mmol, 20%) of isomer 2a as a solid foam and 187 mg (0.50 mmol, 22%) of isomer 2b. Proton NMR spectra correspond to those described earlier [9, 10]. The two reactions recovered 580 mg of the original securinine (pale yellow crystals) during purification.

2.1.3 Method C. Long Reaction with Cerium Chloride

Similarly, from 500 mg of securinine (1, 2.304 mmol), 406 mg of tryptamine in 20 ml of methanol using 87 mg (0.1×, 0.23 mmol) of cerium chloride heptahydrate as a catalyst, a reaction was carried out for 14 days. After purification by column chromatography, 159 mg (0.42 mmol, 18%) of isomer 2a was isolated as a solid foam, as well as 341 mg (0.50 mmol, 39%) of isomer 2b.

2.1.4 Method D. Reaction with Boron Trifluoride Etherate

500 mg of securinine (2.304 mmol), 406 mg of tryptamine (1.1×, 2.534 mmol) were dissolved in 20 ml of dry THF, 142 µl (98%, 0.5×, 1.13 mmol) of boron trifluoride etherate was added dropwise (to prevent the development of blue color), sealed and left at room temperature for 24 hours. After this time, the reaction mixture, a completely transparent yellow solution, was evaporated under reduced pressure, the residue was applied to a silica gel column, eluted sequentially with $CHCl_3$:AcMe:IPA:NEt_3 in a ratio of 40:10:0:0.5, then 40:10:2.5:0.5, 40:15:5:0.5, then $CHCl_3$:AcMe:MeOH:NEt_3 in the ratio 40:15:5:0.5 and 40:15:10:0.5. From fractions f.4-f.7, 404 mg of the original securinine (1) were obtained; fractions f.8-f.10 contained a mixture of reaction products from fractions f.11-f.12, 53 mg of pure isomer B (2b) were isolated from fractions f.13-f.17, 340 mg of a substance identified by NMR as tryptamine were isolated. Fractions f.8-f.10 were rechromatographed in a $CHCl_3$:AcMe:IPA:NEt_3 system with an isopropanol gradient to give 79 mg (0.21 mmol) of isomer A (2a) and an additional 50 mg (0.27 mmol in total) of isomer B (2b) after additional rechromatography.

2.1.5 Method E. Reaction with Copper(I) Chloride

500 mg of securinine (2.304 mmol) were dissolved in 10 ml of acetonitrile, 406 mg of tryptamine (1.1×, 2.534 mmol), 115 mg (0.5×) of cuprous chloride were added, closed, and left at room temperature. TLC monitored the progress of the reaction. After 24 h, a significant amount of the addition product is formed, and at first, only the 2a isomer is detected by TLC. After 4 days, the amount of the 2a isomer increases, but the 2b isomer begins to appear in addition to it. At this point, the reaction mixture was evaporated and applied to a silica gel column. It was eluted with a C_6H_6:AcMe:IPA:NEt_3 mixture with an increasing isopropanol gradient. TLC monitored the composition of the fractions in the C_6H_6:AcMe:IPA:NEt_3 = 15:5:2:0.15 system on silica gel plates (Merck KGaA), detection with anisaldehyde reagent and heating 250°C. In such a system, Rf (2b) = 0.27, orange, after a while purple spots; Rf (2b) = 0.46, orange, after a while purple spots; Rf (3) =

0.60, pink spots. Mixed fractions were rechromatographed in the same system. Yield 2a - 246 mg (0.65 mmol), yellow-brown resin; 2b - 62 mg (0.16 mmol), yellow-brown resin; 3 - 156 mg (0.42 mmol), yellow oil. Substance 3, spectrum ^{1}H-NMR ($CDCl_3$, 500 MHz, δ, ppm., J/Hz): 1.21 (1H, ddd, J = 6.9/3.6/2.8, H4-α), 1.24-1.27 (1H, m, H3-α), 1.38 (1H, dd, J = 9.5/0.9, H8-α), 1.45-1.50 (3H, m, H3-β + H5-α + H5-β), 1.82 (1H, m, H4-β), 2.14 (1H, d, J = 5.6, H14), 2.29 (1H, t, J = 5.1, H15), 2.33 (1H, dd, J = 9.6/4.0, H8-β), 2.60 (1H, dt, J = 11.5/7.5, H1`-α), 2.79 (1H, br.s, H1`-β), 2.89 (2H, m, H6-α + H2), 3.02 (1H, ddd, J = 14.1/7.8/5.6, H2`-α), 3.11 (1H, dd, $J$ = 14.5/7.2, H2`-β), 3.15 (1H, m, H6-β), 3.62 (1H, t, J = 4.3, H7), 5.59 (1H, s, H12), 7.01 (1H, d, J = 2.3, H2``), 7.10 (1H, ddd, $J$ = 9.0/7.0/1.0, H5``), 7.19 (1H, ddd, J = 8.2/6.9/1.2, H6``), 7.39 (1H, d, $J$ = 8.1, H7``), 7.57 (1H, dd, J = 7.9/1.1, H4``), 8.25 (1H, s, NH1``); spectrum ^{13}C -NMR ($CDCl_3$, 126 MHz, δ, ppm): 25.0 (C-4), 25.8 (C-5), 26.1 (C-2`), 28.6 (C-3), 37.6 (C-14), 42.0 (C-8), 47.6 (C-6), 49.7 (C-15), 56.8 (C-7), 61.0 (C-2), 62.2 (C-1`), 90.4 (C-9), 110.8 (C-12), 111.4 (C-7``), 113.6 (C-3``), 119.8 (C-4``), 119.3 (C-5``), 122.1 (C-2``), 122.2 (C-6``), 127.4 (C-3a`), 136.4 (C-7a`), 172.7 (C-13), 173.7 (C-11); LC-MS mass spectrum (ESI) found: m/z 376.35 $[M + H]^+$, calculated for $C_{23}H_{26}N_3O_2$: $[M + H]^+$ = 376.2020.

2.1.6 Method F. Reaction with Copper(I) Chloride

In a vial, 500 mg of securinine (2.304 mmol) were dissolved in 10 ml of dry acetonitrile, 406 mg of tryptamine (1.1×, 2.534 mmol) were added 46 mg (0.2×, 1.15 mmol) of cuprous chloride, suspended in an ultrasound bath, closed and left at room temperature for 4 days. Similarly, the products were isolated by chromatography in the $CHCl_3$:AcMe:IPA:NEt_3 system. The mixed fractions were rechromatographed to pure products several times. Received isomer 2a - 150 mg (0.40 mmol), yellow-brown mass; isomer 2b - 71 mg (0.19 mmol), yellow-brown resin; conjugate 3 - 114 mg (0.30 mmol), yellow resin.

2.1.7 Method G. Reaction with Copper(I) Chloride

In a vial, 500 mg of securinine (2.304 mmol) was dissolved in 10 ml of dry acetonitrile, 406 mg of tryptamine (1.1×, 2.534 mmol) were added, 228 mg (1.0×, 1.15 mmol) of cuprous chloride, suspended in an ultrasound bath, closed and left at room temperature for 46 hours. After this time, the reaction mixture became very dark, and a large amount of products insoluble in chloroform formed. The solvent was distilled off, dissolved in $CHCl_3$:AcMe:MeOH and the residue was loaded onto a silica gel column and chromatographed in $CHCl_3$:AcMe:MeOH:NEt_3 with increasing methanol gradient. Fractions containing the desired products by TLC were combined and rechromatographed to obtain 44 mg (0.12 mmol) of isomer 2a and 90 mg (0.24 mmol) of substance 3 in brownish resin.

2.1.8 Method H. Long Reaction with Silver Nitrate

39 mg (0.1×) of silver nitrate, acetonitrile, 500 mg of securinine (2.304 mmol), and 406 mg of tryptamine (1.1×) were dissolved in the vial, closed, and kept at room temperature for 14 days. After this time, the mixture darkened, and silver fell out on the vial's walls. The mixture was then evaporated and purified by chromatography, as described above. After additional chromatography, 129 mg (0.34 mmol) of isomer 2a, a yellow-brown viscous oil, and 216 mg (0.57 mmol) of isomer 2b, a yellow-brown viscous oil, were obtained.

2.2 Biology

2.2.1 *In vitro*

Antiaggregatory Activity. The effect of the studied compounds on the aggregation of β-amyloid (1-42) was analyzed using the method of recording Thioflavin T fluorescence (10 μM) [15] for 72 hours at 37°C. The fluorescence signal was measured using a multifunctional flatbed analyzer Cytation™3 (BioTek Instruments, Inc., USA) at λ_{ex} = 450 nm, λ_{em} = 480 nm. Data were representative of three independent experiments.

Measurements of β-Secretase 1 (BACE1) Activity. The effect of the studied compounds on the BACE1 enzyme was evaluated using the commercially available BACE1 (β-Secretase) FRET Assay Kit, Red (Pan Vera, USA) by analyzing the BACE1 fluorescent resonance energy transfer. All procedures were carried out following the manufacturer's protocol. A substrate and an enzyme were added to the test substances in compliance with the experimental scheme. After 60 minutes of incubation at room temperature, the fluorescence signal was measured using a multifunctional flatbed analyzer Cytation™3 (BioTek Instruments, Inc., USA) at λ_{ex} = 545 nm, λ_{em} = 585 nm.

2.2.2 Docking

The corresponding structures were found in the PDB protein structure bank for β-amyloid - 1IYT. The structures were loaded and processed with the Protein Preparation Wizard subprogram of the Schrodinger Suite [16-25]: missing loops and side chains, if any, were restored; preprocessing was performed using the Prime module [18-20]. Hydrogen bonds were optimized; non-key water and other non-key small molecules, if any, were removed; limited minimization of protein geometry was performed using the OPLS3e force field [22].

Ligand structures were prepared using the subprogram LigPrep [26]. The initial 'blind' docking into the β-amyloid structure was performed using the Glide SP protocol, involving the entire peptide in the preliminary receptor grid generation procedure. Once the 'active sites' of the peptide were located and correlated with literary data, Induced Fit docking and subsequent Glide MM-GBSA scoring were conducted. Induced Fit docking was initiated using docking poses obtained from Glide SP preliminary 'blind' docking, with a redocking protocol of induced fit procedure also being Glide Standard Precision. The Prime module processed amino acids within 5 Å radius of the ligand atoms based on the results of pre-docking of ligands in the Induced Fit algorithm. Poses attained after Induced Fit Docking were then processed with MM-GBSA subroutine to obtain Gibbs Free energy values. During MM-GBSA calculations, amino acids within 5 Å from the ligand were additionally optimized.

2.2.3 *In Vivo*

Institutional Review Board Statement. All animal work was carried out following the rules of Good Laboratory Practice in the Russian Federation (2016). The Bioethics Committee of IPAC RAS provided full approval for this research (Approval No. 61, dated 18/04/2021 and No. 64, dated 20/06/2021).

Animal Care and Ethics Statement. The Animal Care and Use Committee of Institute of Physiologically Active Compounds of Russian Academy of Sciences approved all animal procedures. For *in vivo* studies, 11-month-old male C57BL6/j mouse line and 11-month-old male mice of the 5xFAD line (Tg(APPSwFlLon, PSEN1×M146L×L286V) 6799Vas/J) were used. The animals were maintained on a 12/12 h light/dark cycle at 23 ± 1°C and 50 ± 5% humidity. Water and food were provided ad libitum for the duration of the experiment.

The same experimenter conducted all the behavioral testing in an isolated room and at the same time of the day. Researchers had a specific qualification for experimentation on live animals.

5xFAD Transgenic Animal Model. Before experiments, animals were randomly divided into three groups (n = 8 per group) as follows: (1) Control group (11-month-old C57BL6/j mouse line); (2) 5xFAD group; (3) 5xFAD + 2b group.

Allomargaritarine was dissolved in saline solution with DMSO (10%) immediately before use and intraperitoneally administered to animals for 21 days at a 15 mg/kg body weight. In the control group and 5xFAD group, the solution (saline and DMSO (10%), intraperitoneal) was administered within the same schedule.

Figure 1 shows its schematic representation to reflect the experiment's protocol visually.

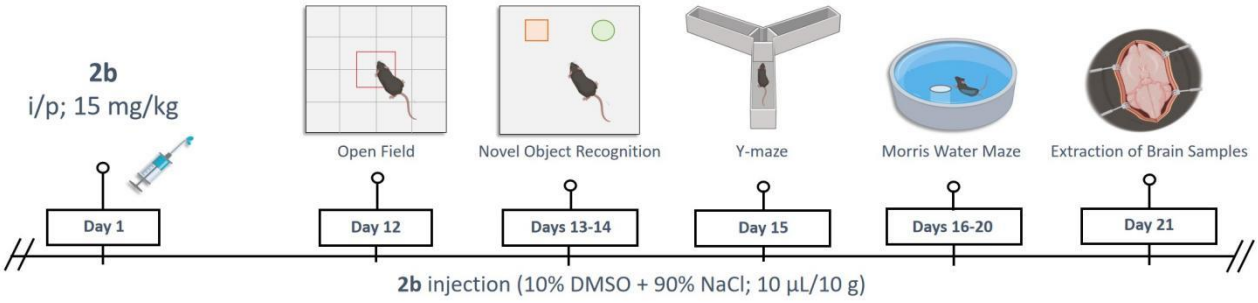

Figure 1 Schematic representation of the *in vivo* experiment protocol.

The Novel Object Recognition Test. Novel object recognition, conducted as previously reported [27], evaluated episodic memory. The lighting conditions were 50 lux. On the first day of the experiment, mice were habituated to an empty square, non-transparent, gray box (40 cm × 40 cm × 40 cm) by allowing them to freely explore the environment for 5 min (no data were collected). The experimental arena was thoroughly cleaned, dried, and ventilated after each animal was treated with 70% ethanol to eliminate the odor cues. After 24 hours, mice were habituated to the chamber with two identical objects, which were localized symmetrically and approximately 10 cm away from the wall for 5 minutes, and then placed in a holding cage. After 24 h, object recognition was tested by substituting a novel object for a familiar training object (the location of the unknown object with the same texture and size but differed in shape counterbalanced across mice). Time spent with each object was recorded and analyzed by a computer-operated EthoVision XT system (Noldus, Wageningen, the Netherlands). The exploration of the objects is considered when a mouse shows any investigative behavior (head orientation or sniffing occurring) or enters an area within 1 cm of the object [28]. Successful memory formation in mice was indicated as a preference for the novel object (significantly more time than spent with the familiar object) because mice inherently prefer to explore unknown objects.

Y-Maze Test. The Y-maze test was used to assess the short-term spatial memory of animals. Test box Y-maze was made of a gray rigid polyvinyl chloride with three arms (arm size 32.5 cm × 8.5 cm × 15 cm) arranged at an angle 120°. The light was supplied from above to ensure a uniform illumination distribution (the intensity was 50 lux). The experiment consisted of two stages. During the training session, mice were allowed to explore two arms of the maze for 5 min. During the testing session (5 min), animals were allowed to explore the entire maze, including the new arm. The time interval between the two sessions was 30 min. All trials were videotaped for post-processing using the EthoVision XT system (Noldus, Wageningen, Netherlands). As a criterion for the effectiveness of memory formation, the duration of the animals' stay in the new arm of the maze during the test was recorded [29].

Morris Water Maze Test. To test hippocampal-dependent spatial cognition, mice were trained in the Morris water maze test with a hidden platform [30].

The circular pool (diameter, 150 cm; height, 60 cm; OpenScience, Russia) of the Morris Water Maze was made of white solid polypropylene with an anti-reflective coating and was filled with tepid water (22 ± 1°C). The lighting conditions were as follows: the dark side of the pool was 50 lux, and the light side was 75 lux. A white escape platform (10 cm diameter) was located 1 cm below the water surface in a fixed position. Distal visual cues in the form of 4 figures (OpenScience, Moscow, Russia), settled on racks and located on the sides of the pool - were available to mice for viewing. All the trials were recorded and traced using a video camera placed above the pool connected to the EthoVision XT system (Noldus, Wageningen, Netherlands). This allowed us to analyze many behavioral parameters. The experiment included two phases during the 5 days.

During the first four training days, they included four trials per day. In each trial, mice were placed at one of the starting locations in random positions (north (N), south (S), east (E), and west (W)) facing the pool wall and were allowed to swim until they located the platform. Mice failing to find the platform within 60 s were carefully guided to it for 30 s (the same period as the successful animals).

Four days after the hidden platform training protocol was completed, probe trials were performed on the fifth day of the experiment to test spatial memory retention. The platform was removed from the pool in the probe session, and mice were allowed to swim for 90s. The time spent in the trained and non-trained quadrants, the number of entrances to the platform area, and the latency period of entering the platform area were recorded [31]. As indicators of locomotor activity, the average speed of movement and the distance traveled were recorded.

2.3 Ex vivo

At the end of the *in vivo* experiments, the animals' brains were sampled to further measure the lipid peroxidation level and glutathione content in mouse brain homogenates. As described below, a synaptosomal p2 fraction containing mitochondria was also isolated to investigate bioenergetic characteristics.

2.3.1 MDA Level and Glutathione Content

The intensity of lipid peroxidation of the mouse brain homogenate was determined using the thiobarbituric acid reactive substances (TBARS) method without initiators [11]. The performance of

the glutathione (GSH) system of the cell's antioxidant defense was evaluated using a commercially available kit (Glutathione Assay Kit, Sigma Aldrich) following the protocol provided by the manufacturer. The total glutathione level was determined by spectrophotometric measurement at a wavelength of 412 nm by the amount of 2-nitro-5-thiobenzoic acid, a product formed during the reduction of GSH 5,5'-dithiobis-(2-nitrobenzoic acid).

2.3.2 Bioenergetic Characteristics of the Mitochondria

The activity of electron transport chain complexes was assessed in preparation of the mitochondrial p2 fraction of the brain (10 µg/well) using the Agilent Seahorse XF96e Analyzer (Seahorse Bioscience, USA) to measure the rate of oxygen uptake triggered by modulators as described early [32]. For this purpose, the activators of the electron transport chain complex I - glutamate/malate, the inhibitor of the complex I - rotenone (2 µM), the substrate of the difficult II - potassium succinate (2 µM), the inhibitor of the complex III - antimycin A, and the substrates of the complex IV - 0.5 µM ascorbate/tetramethyl-p-phenylenediamine (TMPD) were used.

2.3.3 Histology and Histochemistry

The mouse brain was fixed in 10% neutral buffered formalin (Leica Biosystems Inc., USA) for histological examination at +4°C for 24 hours. Then the material was dehydrated, defatted and clarified using ethanol-xylene wiring according to the following scheme: deionized water (2 h); 70% ethanol (12 h at +4°C); ethanol 96% sequentially (15 min, 4 stages × 10 min each); a mixture of ethanol and xylene 1:1 (30 min); xylene (2 stages × 30 min each, 18 h at +4°C); paraffin (3 times × 1 h each). Then, the paraffin-embedded material was processed using a Leica EG1160 apparatus (Leica Biosystems Inc., USA). Paraffin blocks were cut using a Leica RM 2265 rotary microtome (Leica Biosystems Inc., USA), section thickness 8 µm, and mounted on Leica X-tra Adhesive glasses (Leica Biosystems Inc., USA) with poly-lysine. Dewaxing was done using a Leica ST 5020 robot (Leica Biosystems Inc., USA) according to the scheme: 3 times xylene for 10 min each, 2 times 96% ethanol for 15 min each, 75% ethanol for 10 min, then distilled water for 10 min [33, 34]. Following this, dewaxed sections were subjected to histochemical staining to visualize β-amyloid aggregates. The following staining scheme was adopted: Congo Red (Sigma Aldrich, USA) for 5 min, tap water for 5 min, Mayer's hemalum (Potassium hydroxide (Sigma Aldrich, USA) in 80% ethanol (100 ml) for 5 min, tap water for 10 min [35]. The stained sections were embedded under coverslips using Immu-Mount (Thermo Shandon Ltd, UK). The resulting staining was evaluated using a ZEISS LSM 880 laser scanning microscope with an Airyscan module (Carl Zeiss Vision, Germany). Image acquisition was carried out at the same settings, using the "tile scan" function of the microscope. Images were processed using ImageJ 1.52 (1.8.0_172). A 10 × 10 grid was imposed on images containing only brain tissue. In 10 grid cells located obliquely from the top left to the bottom corner [36], selected plaques were assessed using the "magic wand" tool to calculate the average plaque’s area. Three images were analyzed with a microscopic power field (5 inches) for each animal in each group, then averaged for three animals in a group.

2.4 Data Analysis

During the *in vivo* experiments, none of the animals have been excluded from any group. The data was expressed as mean ± SEM. Statistical comparisons were made using analysis of variance (ANOVA) followed by Bonferroni post hoc tests. Two-way repeated measures (mixed model) ANOVA followed by Bonferroni posttests were also used to compare the recognition of two objects during the cognitive assessment. The data analysis for the *ex vivo* experiments was evaluated using a one-way analysis of variance (ANOVA) followed by Dunnett's Multiple Comparison tests. A difference with p value ≤ 0.05 was considered statistically significant. The statistical analysis was performed using GraphPad Prism 5 (GraphPad Software, San Diego, CA, USA).

3. Results

3.1 Chemistry

Starting from securinin (1), the products of its Michael addition with tryptamine at the double bond at position Δ^{14} were synthesized. The use of a ytterbium triflate catalyst leading to stereospecific addition (Table 1, Methods A and B) did not produce allomargaritarine as the only reaction product. Instead, two possible epimers of 15-*epi*-allomargaritarine 2a and allomargaritarine 2b proper were formed at once in an approximately equal ratio. The reaction rate in this variant is extremely low, 14 days of reaction were required to achieve acceptable yields of 2b. It is assumed that $Yb(OTf)_3$, as a Lewis acid, coordinates the lactone cycle in the securinine molecule, which promotes the 1,6-Michael addition (Figure 2). Replacing the catalyst with cerium (III) chloride (method C) led to almost identical results. Replacing the reaction solvent with aprotic THF and the catalyst with boron trifluoride (method D) led to a significant formation of products already after a day of reaction.

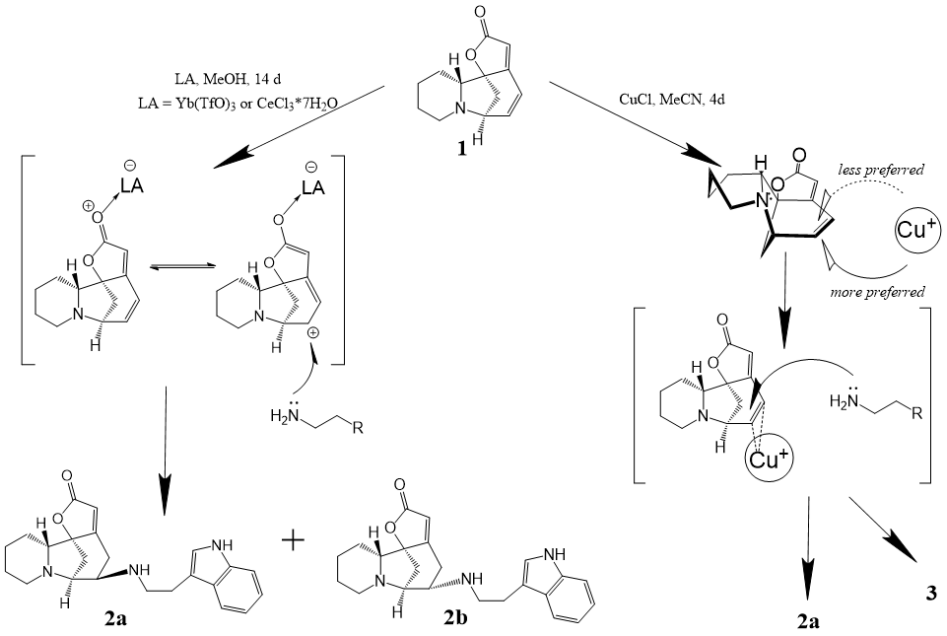

Figure 2 Two approaches to the synthesis of securinine-tryptamine conjugates using Lewis acids.

Table 1 Dependence of allomargaritarine isomer formation depending on reaction conditions.

	Catalyst, solvent	Catalyst Excess	Time	Yield 2a (%)	Yield 2b (%)	Yield 3 (%)
A	$Yb(OTf)_3$, MeOH	0.1	6 d	-[a]	20	-
B	$Yb(OTf)_3$, MeOH	0.1	14 d	20	22	-
C	$CeCl_3 \times 7H_2O$, MeOH	0.1	14 d	18	39	-
D	$Bf_3 \times Et_2O$, THF	0.5	24 h	9	12	-
E	CuCl, MeCN	0.5	4 d	28	7	18
F	CuCl, MeCN	0.2	4 d	17	8	13
G	CuCl, MeCN	1.0	46 h	5	-	10
H	$AgNO_3$, MeCN	0.1	14 d	15	25	-

a - The product was not isolated.

Another approach to synthesizing allomargaritarine involves using securinine in an amino addition as an unactivated alkene that forms complexes with mild Lewis acids. When used as a catalyst (procedures E-G) in reaction with securinine (1), copper monochloride leads to a faster tryptamine addition reaction. Moreover, the kinetically preferred isomer 2a is predominantly formed in this variant. After a day of reaction with CuCl, the formation (according to TLC) of only isomer 2a is observed, and only after several days does the target isomer 2b begin to form in noticeable amounts. The reaction, in this case, does not stop at the formation of amino conjugates 2a and 2b; product 3 is also formed in significant amounts, for which, based on 2D NMR, the structure (Figure 3) of the conjugate of securinine and tryptamine connected through an aziridine bridge was established. Comparing the triplet signal in aziridine at the H-7 atom with the described multiplets in the spectra of isomers 2a and 2b [10], we can conclude that substance 3 corresponds to the 2a isomer with an additional bond. Although low stability can be expected from aziridines, substance 3 became even more stable in air than amino conjugates 2a and 2b.

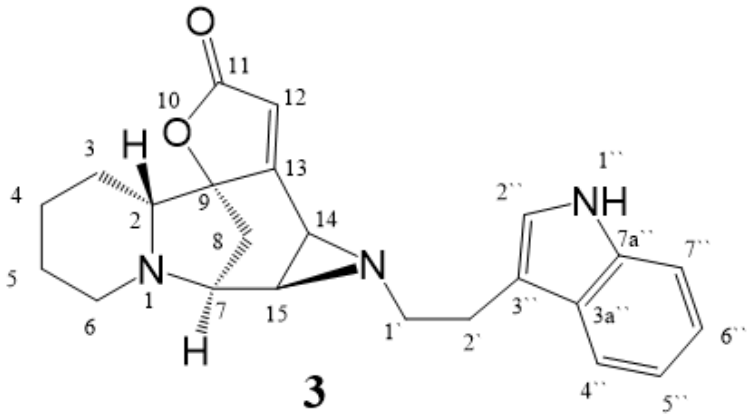

3

Figure 3 The structure and atomic numbering of the by-product in the synthesis of allomargaritarine.

3.2 Biology

3.2.1 Influence of 2b on BACE1 Activity and $A\beta_{1-42}$ Aggregation

In an *in vitro* study of the biological activity of 2b, the effect of the compound on the processes associated with β-amyloid homeostasis was analyzed. As shown in Figure 4A, 2b at a concentration of 100 µM, similar to the reference compound GL189, significantly reduced the activity of BACE1, which was not found for parent substances securinine (1) and tryptamine (Tr). The half maximal inhibitory concentration (IC_{50}) for 2b was 58.12 ± 0.12 µM (Figure 4B). Moreover, unlike the original compounds, 2b effectively suppressed the aggregation process for 72 hours (Figure 4C), and this effect was concentration-dependent (Figure 4D). Thus, 2b effectively inhibits BACE1, a critical enzyme that triggers the amyloidogenic APP cleavage pathway and prevents the aggregation of pathological $A\beta_{1-42}$.

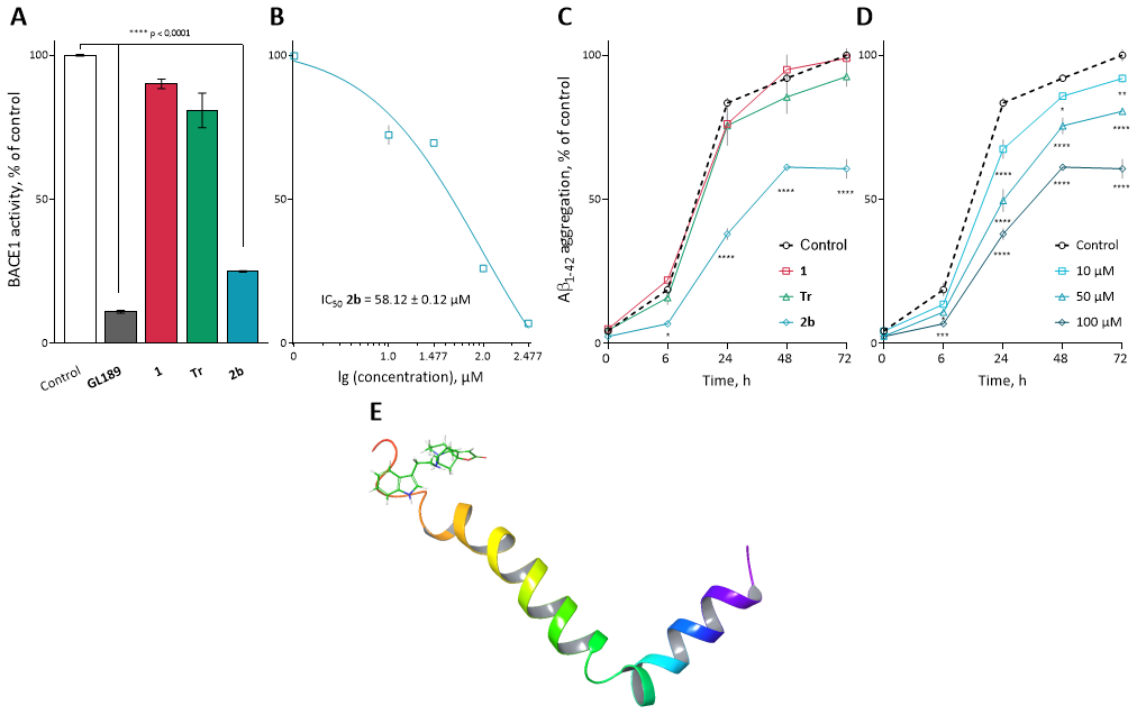

Figure 4 Inhibition of BACE1 enzymatic activity and Aβ aggregation by 2b. **A** - Effect of test compounds at a concentration of 100 µM on BACE1 activity. The BACE1 concentration was 1.0 U/ml. Data are presented as mean ± SEM (n = 3). ****, $p \leq 0.0001$ versus Con (one-way analysis of variance (ANOVA) followed by Dunnett's multiple comparison tests). **B** - Effect of 2b on BACE1 enzymatic activity. The concentration range of the substance was from 1 to 100 µM. Based on the dose-dependent curves, the concentration values leading to 50% inhibition of BACE1 activity (IC_{50}) were calculated. **C** - ThT fluorescence curves in the presence of test compounds at a concentration of 100 µM; **D** - concentration-dependent inhibition of $A\beta_{1-42}$ aggregation by 2b; concentration range from 10 to 100 µM. *, **, ****, $p < 0.05$, $p < 0.01$ and $p < 0.0001$ *versus* Control. The statistical analysis was performed using two-way ANOVA and the Bonferroni test. **E** - Overlay of the structure of the 2b - protein molecule for the results of free compound docking into β-amyloid.

A docking procedure was performed to confirm the effect of substances on β-amyloid aggregation (Table 2), which is an exceptional alternative to expensive and inaccessible transmission electron microscopy methods. The accessible structure of PDB ID 1IYT was obtained by NMR spectroscopy and contained ten monomer conformations. The structure was unloaded and processed by the Protein Preparation Wizard subroutine of the Schrodinger Suite software package: missing loops and side chains, if any, were restored; preprocessing was performed using the Prime module. Hydrogen bonds were optimized, water molecules and other small molecules were removed, and limited minimization of the protein geometry was performed (OPLS3e force field). The ligand structures were prepared using the LigPrep subroutine, several biologically possible protonated structures were obtained for 2b, and their pKa was estimated using the Jaguar subroutine.

Table 2 Results of 2b binding to β-amyloid peptide.

Compound	Hydrogen bonds	Other interactions	ΔG_{bind} (MM-GBSA, kcal/mol)
2b - Azepine protonated	GLU3 ASP7 GLU11	Salt bridge: ASP7 GLU11	-3.844
2b - Linker protonated	GLU3 GLU11	Salt bridge: GLU11	-3.372
2b - Neutral	GLU3	Pi-Pi stacking: TYR10	-3.267
2b - Diprotonated	GLU3 ASP7	Salt bridge: GLU3 ASP7 GLU11 Pi-Pi stacking: TYR10	-1.539

To determine the binding pockets, blind docking was initially performed across the entire peptide surface. Analysis of the obtained results indicates the two most energetically favorable binding pockets: near the C-terminal end of the peptide and in a bend near the N-terminal end of the peptide, which agrees with literature data [37, 38]. After refining the coordinates of the binding pockets, MM-GBSA calculations were performed, and an estimate of the binding Gibbs energy for 2b at both positions was obtained. The binding Gibbs energy estimate was used to calculate the relative probabilities of realizing a particular docking pose for a given substance.

Figure 4E visually identifies the binding position of the neutral form of 2b directly to β-amyloid. Thus, it was found that 2b exhibits the ability to inhibit the aggregation of Aβ through interaction with the N-terminus of the protein.

3.2.2 Neuroprotective Effects of 2b in an *In Vivo* Testing

As part of the *in vivo* study of the neuroprotective potential of 2b, we conducted a comprehensive analysis of the effect of the compound on various types of memory. Initially, we evaluated the function of long-term episodic memory in the Novel Object Recognition test based on the analysis of the preference of a novel object in a test trial.

Figure 5A shows the percentage of time spent learning about two objects (familiar and novel) by experimental groups during the testing phase. Thus, transgenic mice that did not receive 2b treatment showed a deficit in cognitive behavior, defined as a decrease in preference for a novel object compared to a familiar one (56.59 ± 5.31 seconds for an everyday object and 43.41 ± 5.31 seconds for an unknown object). Clinically healthy mice and the 5xFAD group of animals treated with 2b showed a typical preference for a new object when recognizing objects, while only for the

5xFAD + 2b group this indicator was significantly increased from (39.09 ± 2.28 seconds for the familiar object and 60.91 ± 3.28 seconds for the novel object, p = 0.01).

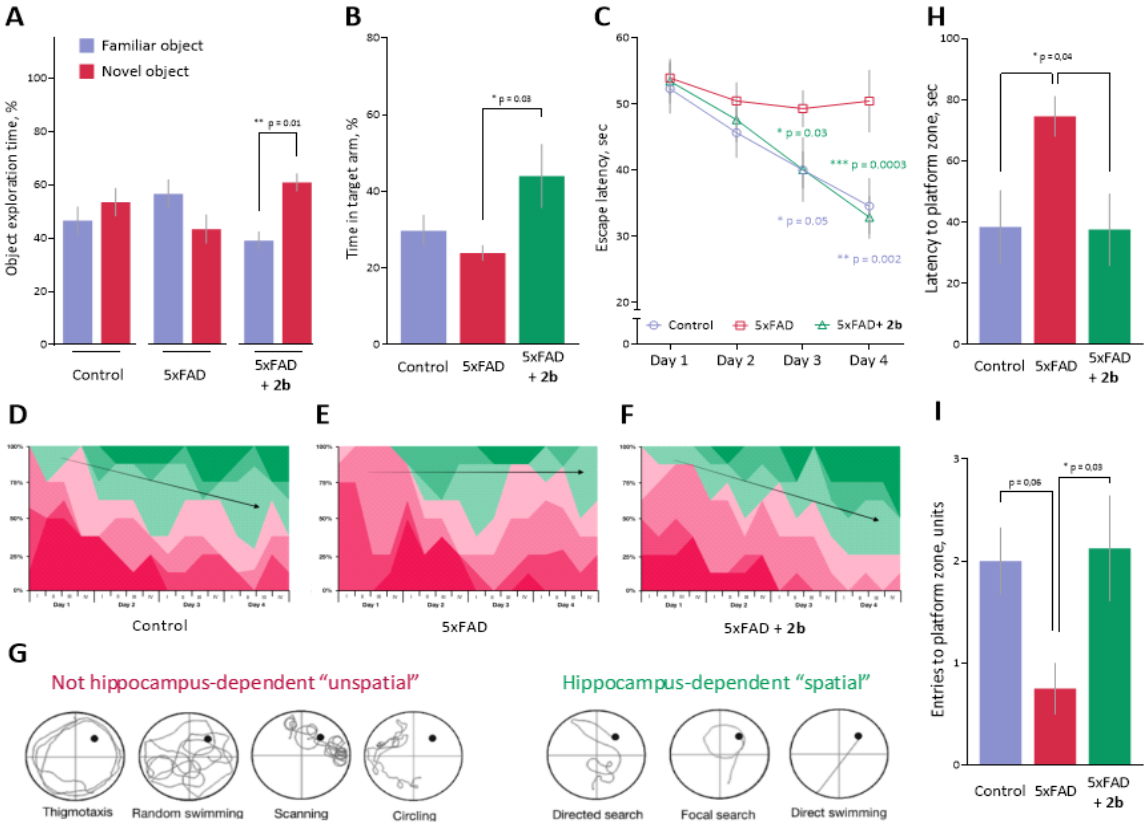

Figure 5 Neuroprotective effects of 2b in an *in vivo* series of experiments in 5xFAD transgenic mice. **A** - effect of 2b on episodic memory of mice in the Novel Object Recognition Test. **B** - effect of 2b on spatial memory formation in mice assessed using Y-Maze Test. **C** - effect of 2b on learning and spatial memory of mice using Morris Water Maze training test. **D-G** - effect of 2b on progression toward hippocampus-dependent search strategies of mice in the Morris Water Maze training phase. Hippocampus-independent egocentric navigation includes several types of target-seeking strategies: (1) thigmotaxis - the animal moves only along the periphery of the arena; (2) random search - the animal begins to move away from the periphery of the arena with visible movements inward; (3) scanning - behavior associated with random search, focused on the center of the swimming pool; (4) circling - disorderly swimming of the animal in circles. Hippocampus-dependent allocentric orientation includes (1) directed search - swimming with small circular or winding movements to find a platform; (2) focal search - this behavior is also associated with random searches, but here, an animal is actively looking for a specific small section of the arena; (3) direct swimming - an animal goes directly to the platform. **H-I** - effects of 2b on spatial memory of mice using Morris Water Maze Probe Trial. Data are presented as mean ± SEM (number of animals in each group, n = 8). **A** - **, $p < 0.01$, versus familiar object. **B** - *, $p < 0.05$, versus 5xFAD. **C** - * $p < 0.05$, ** $p < 0.01$, *** $p < 0.001$, **** $p < 0.0001$, versus 1st day of training. **H-I** - *, $p < 0.05$ versus 5xFAD. The statistical analysis was performed using two-way ANOVA and the Bonferroni and Dunnet tests.

In the next step, we evaluated the impact of 2b on social learning and short-term memory in 5xFAD mice in the Y-maze test. As shown in Figure 5B. During the testing phase, animals from the 5xFAD group demonstrated an expected decrease in the time spent in the novel, a previously unexplained maze arm (23.91 ± 1.97 seconds). However, mice from the 5xFAD + 2b group demonstrated significantly higher values of this indicator (43.99 ± 8.27 seconds, p = 0.03 compared to 5xFAD, Figure 5B).

We also evaluated the effect of 2b on learning and the formation of long-term spatial memory in the Morris water maze test. As shown in Figure 5C, compared to controls, the 5xFAD group showed no changes in the escape latency (swimming time for mice to find the platform) up to the fourth experimental day. Such duration of the aimless swimming suggests that both transgenic mice exhibited impaired spatial memory.

Notably, clinically healthy outlandish animals and mice treated with 2b showed a significantly improved learning pattern. So, on the third day of the experiment, this indicator was significantly reduced by 23.44% (control group) and 24.93% (5xFAD + 2b), and on the fourth day - by 33.92% (Control group) and 38.44% (5xFAD + 2b).

Additionally, we analyzed the strategies for hidden platform search by animals during the entire training period [39]. The approach logic is linked to the gradual switching of the hippocampus-independent egocentric navigation (shades of pink), observed in the first days of placing the animal in the installation, to the hippocampus-dependent allocentric (shades of green) pattern with the addition of various motion vectors using distal cues (visual cues located at the sides of the pool, Figure 5G). During the initial phase, the mouse demonstrates a stereotypical sequence of hidden platform search patterns, focusing only on proximal and internal signals. In 5xFAD mice (Figure 5E), the advantage of using hippocampus-independent egocentric navigation was observed up to the last fourth day of training, compared to wild-type clinically healthy animals (Figure 5D). At the same time 2b treatment led to the normalization of responses and the successful formation of an allocentric cognitive map (Figure 5F), which is not different from data collected in the control group.

The successful hippocampus-dependent spatial learning and long-term memory formation were also confirmed during the testing phase on the fifth day of the Morris Water Maze experiment. In the spatial probe trial, in transgenic AD animals, 2b treatment increased the number of entries into the platform zone (Figure 5H). It significantly reduced the latent period of entry into the platform zone (Figure 5I).

3.2.3 Effects of 2b Detected *Ex Vivo*

At the end of the *in vivo* experiments, a *post-mortem* analysis of animal brain samples from experimental groups was performed. As shown in Figure 6A, lower GSH levels were observed in the brain tissues of 5xFAD mice compared to the brain tissues of wild-type mice (p = 0.001), while treatment with 2b significantly increased this indicator. A similar situation was observed with MDA content (Figure 6B). MDA was substantially higher in 5xFAD mouse brains (1.17 ± 0.014 nmol/mg protein) compared to the control group (0.94 ± 0.015 nmol/mg protein). However, the 2b treatment significantly reduced MDA levels in 5xFAD mice (0.71 ± 0.01 nmol/mg protein).

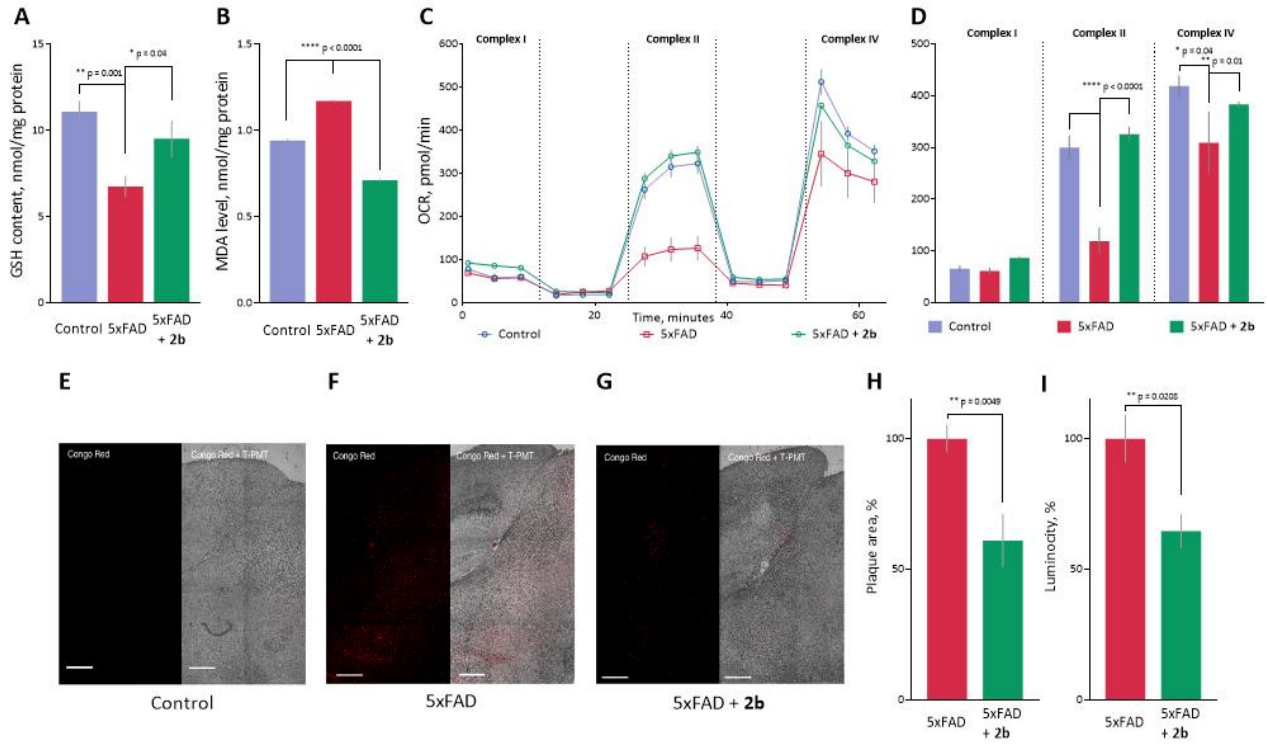

Figure 6 *Ex vivo* analyses of post-mortem brain samples of 5xFAD transgenic mice. **A** - analysis of GSH content and **B** - MDA level. **C-D** - analysis of the activity of the electron transport chain complexes in mice's brain mitochondria. Rotenone concentration is 2 µM, potassium succinate - 2 µM, antimycin A - 4 µM, ascorbate/TMPD - 0.5 µM. **E-G** - microphotographs are shown and indicate mice brain sections labeled with Congo Red to visualize Aβ deposits and T-PMP signal to identify the morphology (white scale bar denote 500 µm) and percentage of brain tissue area covered by plaques - **H** - and its luminosity - **I**. Data are shown as mean ± SEM. * $p < 0.05$, ** $p < 0.01$, **** $p < 0.0001$ *versus* 5xFAD. The statistical analysis was performed using two-way ANOVA and the Dunnet test.

When studying the functioning of electron transport chain complexes in the mitochondrial p^2 fraction, we found that in samples of 5xFAD transgenic animals, a reduced rate of oxygen consumption is observed due to impaired electron transfer through succinate and ascorbate/TMPD (Figure 6C, 6D). In turn, the oxygen consumption rate was increased in transgenic animals treated with 2b. So, after succinate administration, 2b increased the OCR in transgenic mice from 119.07 ± 25.51 pmol/min to 325.69 ± 13.74 pmol/min ($p < 0.0001$), at the same time after administration of ascorbate this indicator was also increased from 308.78 ± 59.54 pmol/min up to 383.08 ± 5.05 pmol/min ($p < 0.01$) (Figure 6C, 6D).

Moreover, to assess the 2b ability to influence the deposition of Aβ plaques, we stained mouse brain sections with Congo red, which labels the amyloid core of mature plaques. Positive staining was found in both 11-month-old transgenic AD mice groups but not in wild-type animals (Figure 6E-6G). Notably, there was a significant decrease in the area of β-amyloid aggregates ($p = 0.0049$) and luminescence intensity ($p = 0.0208$) in the brain in mice treated with 2b, compared to 5xFAD (Figure 6H-6I).

4. Discussion

4.1 Chemistry

To obtain allomargaritarine, we took its synthesis as a starting point based on more accessible components - tryptamine and natural alkaloid securinine [10]. It was stated that in methanol, the addition of an amine at the double bond of securinin occurs to form two epimers, and the use of Yb(OTf)3 as catalyst leads to the formation of 2b as the single isomer. The formation of two isomers at once complicates the purification of products into individual substances. But, more importantly, the reaction proceeds very slowly in this embodiment. At first glance, it seems that it does not occur at all. Thus, after a day of reaction, only traces of products are detected, and it takes 14 days to achieve at least acceptable yields. It is assumed that the reaction proceeds along the 1,6-Michael addition pathway, and in this case, the coordinating force of Yb(OTf)3 on the carbonyl in the lactone ring may be insufficient. Replacing the Lewis acid with cerium (III) chloride, another oxyphilic lanthanide, led to similar results, requiring a long reaction time and a mixture of product isomers. Perhaps methanol as a protic solvent is an unfortunate choice for use with Lewis acids. In this case, catalysis does not occur at all since the same mixture of products is formed [10] in pure methanol without the addition of $Yb(OTf)_3$. Using aprotic THF as a solvent and boron trifluoride as another classical Lewis acid catalyst soluble in non-polar solvents significantly increased the reaction rate. In past cases, catalysis was possibly ineffective precisely because the protic solvent or bound water (in the cerium method) inactivated the Lewis acids.

Another approach to the synthesis of allomargaritarine is possible. Since the addition of tryptamine follows the 1,6-way, the double bond, in this case, experiences only a weakened activating effect of the lactone ring. Therefore, it is possible to use securinine in the reaction as a non-activated alkene, giving complexes with mild Lewis acids such as copper chloride (I). This approach has the advantage of a higher reaction rate with the predominant formation of one of the reaction products, which is associated with the preferable formation of one of the forms of the securinine-copper complex formed in the first stage. The disadvantage of the second approach is the formation of a large number of by-products, mainly due to the oxidation of tryptamine.

4.2 Biology

Alzheimer's disease (AD) is a highly complex and widespread neurodegenerative disease that has not yet been thoroughly studied and is not subject to radical treatment but only symptomatic correction. Today, Alzheimer's disease is the seventh leading cause of death in the world, with more than 55 million people with the disease. According to the International Federation of Associations against Alzheimer's Disease and dementia, Alzheimer's Disease International (ADI) 131.5 million cases of the disease are expected worldwide by 2050 [40]. It dictates the need for new approaches to creating promising next-generation medicines.

The pathogenesis of Alzheimer's disease has been the subject of intensive research for several decades, so today, there are a large number of hypotheses about the molecular causes of Alzheimer's disease, among which the most common theory focuses on the pathology of amyloid formation [38, 39]. The toxic role of senile plaques was discovered by Alois Alzheimer almost 110 years ago [40], and today, a wide range of pathological cascades caused by this phenomenon has

been convincingly proven [41], in particular, dysfunction and significant loss of neurons in some regions of the brain (mainly the parietal and temporal cortex, as well as the hippocampus) [42].

According to the current state of the amyloid hypothesis, therapy aimed against Alzheimer's disease requires the development of new multimodal strategies. Such drugs should simultaneously prevent the aggregation of this toxic protein and inhibit the enzymes involved in the formation of β-amyloid peptide to dispose of pathological fragments [43, 44].

It is well known that the initial formation of β-amyloid peptide occurs due to cleavage of the C-terminal part of the amyloid precursor protein by secretases (alpha, beta, and gamma) [42]. The enzyme that generates pathological forms of β-amyloid peptide 1-40 and 1-42 is β-secretase 1 (β-site amyloid precursor protein-cleaving enzyme-1, BACE 1) [45]. Thus, since the discovery of this enzyme more than 20 years ago, much has become known about its structural features and physiological functions, making it the primary therapeutic target for inhibiting the production of Aβ in Alzheimer's disease.

Inhibition of β-secretase 1 is a modern and promising approach to combat β-amyloid (Aβ) deposits in the brain of patients with Alzheimer's disease [46]. To date, there are already several modulators of the activity of this enzyme, clinical trials of which, unfortunately, have not yet been successful due to insufficient efficacy or pronounced toxicity. Thus, the high efficacy of atabecestat (JNJ-54861911) shown in the early research stages could not allow the further introduction of this agent into clinical practice due to the pronounced hepatotoxicity detected for it in phase III clinical trials [47]. Phase III studies of the BACE 1 inhibitor lanabecestate for the treatment of prodromal stages of Alzheimer's disease were discontinued due to lack of clinical benefit [48].

Nevertheless, because BACE 1 is an excellent therapeutic target due to its direct participation in the formation of toxic forms of β-amyloid peptides and, as a result, neurodegeneration, BACE 1 inhibitors are considered valuable pharmacological tools in the fight against the critical pathogenetic event of Alzheimer's disease - β-amyloid proteinopathy.

In our work, we conducted a study of the BACE 1 inhibitory activity of allomargaritarine (2b), which is considered one of the possible mechanisms of the neuroprotective action of the compound. Thus, the modulation of BACE 1 by 2b was confirmed by in vitro experiments, where using the fluorescence resonance energy transfer method it was found that in the presence of 100 μM 2b, the activity of the recombinant enzyme decreased almost to the level of the reference compound GL189 - commercially available β-secretase inhibitor (H-EVNstatineVAEF-NH2, β-secretase III inhibitor, Calbiochem, Sigma Aldrich) used was as a positive control to confirm the validity of the method and correct performance. The IC_{50} value was 58.12 ± 0.12 μM. This suggests that 2b can implement its neuroprotective potential due to the inhibition of β-secretase 1.

In addition, as mentioned above, therapy aimed at the utilization of directly formed Aβ is the focus of attention of researchers engaged in the development of therapeutic approaches for the treatment of Alzheimer's disease. Many attempts have been made to develop targeted agents aimed at Aβ aggregation, including inhibition of Aβ monomer aggregation, removal of amyloid aggregates, and immunotherapy. However, despite all the efforts made, progress in the effective treatment of Alzheimer's disease and the creation of therapeutic agents in this area is still limited.

To determine whether 2b can directly affect amyloidogenesis, we tracked the aggregation of the pathological β-amyloid peptide 1-42 by assessing the thioflavin T fluorescence signal in the presence of various 2b concentrations. Being a widely used specific marker of amyloid formation, Thioflavin T binds to β-sheets of amyloid fibrils, resulting in an amplification of the fluorescence signal [49],

which was confirmed in our work in control samples. Interestingly, 2b significantly influenced the formation of amyloid aggregates, as evidenced by the absence of pronounced changes in the values of thioflavin T fluorescence. Moreover, we found that the aggregation process of β-amyloid strongly depended on the concentrations of the compound under study. Thus, the final value of thioflavin T fluorescence at the end of the 72-hour incubation period in samples with the maximum studied concentration of 2b 100 µM decreased to an intensity approximately twice lower (by 40.4%) than in control samples, with a decrease of this indicator by 8.1% and 19.4% at 10 µM and 50 µM, respectively.

Therefore, we have discovered that a side from the previously reported antioxidant, cytoprotective and cytoprotective activities [11], 2b equally effectively inhibits BACE1. This key enzyme triggers the amyloidogenic APP cleavage pathway, directly preventing aggregation of the pathologic form of β-amyloid peptide 1-42, making this compound a promising agent for proteinopathy in AD. Therefore, 2b may be considered as a potential medicinal agent to combat pathological AD conditions. In vivo tests were conducted with laboratory animals using AD model to confirm this assumption.

The neuroprotective potential of 2b was evaluated for its ability to influence animal cognition in a transgenic AD animals. Preliminarily we have shown that the injection of 2b (up to 300 mg/kg) does not cause deviations in behavioral and physiological responses [13]. This finding allowed us to continue the *in vivo* study of its neuroprotective properties in animals.

In vivo studies used 11-month-old male C57BL6/j mouse line and 11-month-old male mice of the 5xFAD line. The full set of AD pathological conditions was reproduced in the genetically modified line of mice 5xFAD (Tg(APPSwFlLon, PSEN1×M146L×L286V) 6799Vas/J) at 11 months of age [50], including the accumulation of intracellular β-amyloid and its deposits, neuronal death and neurodegeneration [50] (Figure 7).

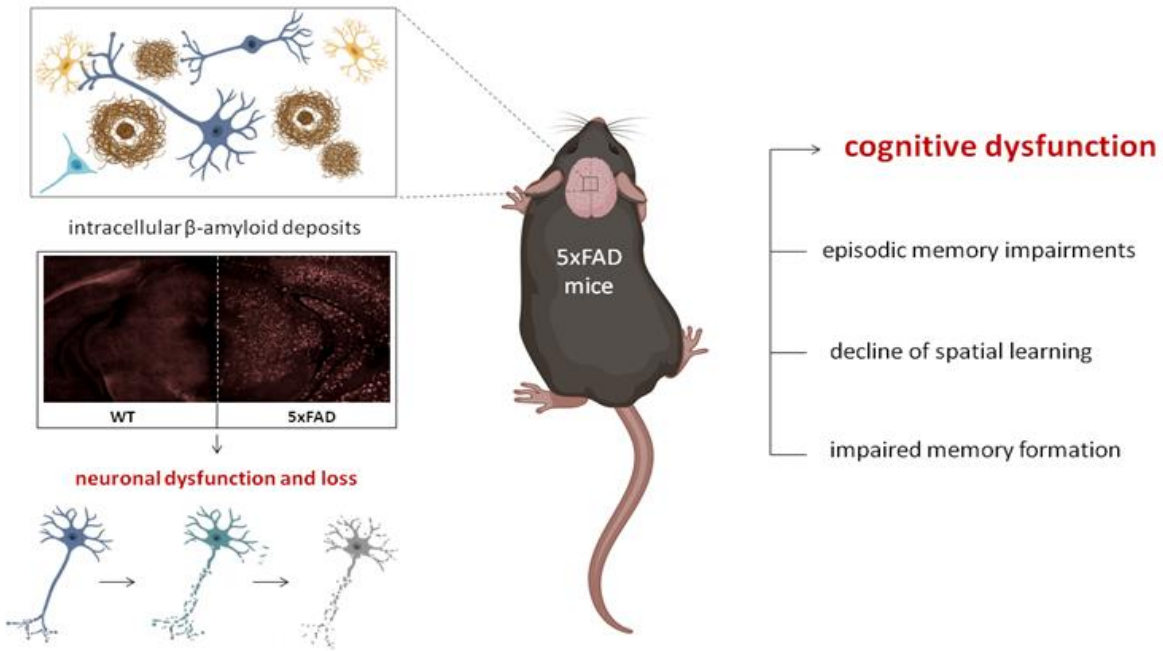

Figure 7 Pathological accumulation of intracellular β-amyloid and its deposits lead to cognitive dysfunction in transgenic AD model mice 5xFAD.

In this study, behavioral tests included a step-by-step analysis of various types of memory, accounting for the differences in the time of storing material (short-term and long-term) and the processes of memorizing, storing, and reproducing information (episodic and spatial).

We assessed the episodic memory of animals in the Novel Object Recognition test. It is known that rodents prefer to explore novel objects longer than familiar ones [51]. Successful memory is formed during the testing phase if the mouse learns about a new object more. We found that in the 5xFAD group, there was no statistically significant difference in the time of exploration of novel and familiar objects ($p > 0.05$), which indicates the absence of successful learning and cognitive dysfunction in mice and is consistent with a large amount of literature data describing this model [52]. This is because this model reproduces neuronal death directly in the brain's hippocampal region. At the same time, the memory assessed in this test is mediated by mechanisms highly dependent on the hippocampus. However, clinically healthy wild-type animals and transgenic mice treated with 2b showed an increased time preference for the novel object. Although in control mice, the difference in this parameter was not significant, which is related to age-related disorders in animals, the time to explore novel objects was significantly longer than that for familiar objects in mice from the 2b treated group ($p = 0.006$).

Then, we investigated the effect of 2b on the spatial memory of mice. The Y-maze test assessed short-term spatial memory, which is based on the innate instinct of rodents to explore an unknown environment [53]. An indicator of the effectiveness of memory formation in this test is the duration of stay of mice in a novel, previously unexplored arm of the maze. In this experiment, a significant decrease in the duration of stay of intact transgenic mice simulating Alzheimer's disease in the new arm of the maze during the testing phase was found, which correlates with the data already known for this model [54, 55]. Interestingly, this indicator was significantly higher in mice treated with 2b ($p = 0.03$). It suggests that treatment with 2b for three weeks restored the short-term spatial memory of 5xFAD animals at 11 months.

The Morris water maze test was used to assess the long-term spatial memory of mice. This test is the gold standard of a behavioral experiment that allows analyzing this type of memory [56]. A significant reduction in the time spent searching for a platform hidden underwater during the training period was observed in clinically healthy wild animals and mice treated with 2b. So, the mice of these groups showed a fast learning curve in the Morris water maze test, with a significant improvement on the third day of the experiment. Moreover, on the fifth day, during the Probe Trial session for the 5xFAD + 2b mice group, a significant increase in the number of entrances to the platform area and a reduction in the time spent searching for the platform area up to the level of the control group were also shown. Thus, in this test, we could convincingly prove and once again confirm the ability of 2b to improve spatial memory dependent on the hippocampus in 5xFAD mice - one of the most affected areas of the brain in Alzheimer's disease [57, 58].

To confirm the neuroprotective potential of 2b, brain samples were taken at the end of in vivo experiments, and the effect of 2b on parameters potentially related to the properties detected for this agent was evaluated.

Because oxidative stress and mitochondrial dysfunctions play a vital role in the pathogenesis of Alzheimer's disease, and antioxidant properties were previously identified for 2b [11], we analyzed the effect of 2b on GSH and MDA levels in brain samples. Thus, it was found that 5xFAD transgenic mice had higher levels of free radicals and impaired functioning of the glutathione link of their

antioxidant defense system, which indicates severe cellular damage. In turn, 2b managed to normalize this situation, aiming for the indicators of clinically healthy mice.

The potential association of 2b with amyloid pathology was investigated by observing the amyloid plaque load in brain tissues of 5xFAD mice. Staining sections of animal brain tissue with a Congo-red label, which detects both compact and diffuse deposits, made it possible to find a typical staining pattern for mice of this age [59]. In mice treated with 2b, there was a significant decrease in the area of deposits and the intensity of staining, indicating that the amyloid plaque burden was lessened.

Using the Seahorse Bioanalyzer, we also evaluated the functioning of brain mitochondria (the activity of respiratory chain complexes). Significantly lower oxygen consumption was found in transgenic 5xFAD animals compared to clinically healthy mice after injections of succinate and ascorbate/TMPD (II and IV complexes). This suggests that the electron-transport chain is functionally different in 5xFAD mice and may explain higher levels of malondialdehyde in the brain due to the increased formation of reactive oxygen species. In turn, in the samples of animals treated with 2b, a typical curve of change in the rate of oxygen consumption by organelles with the addition of modulators was revealed, similar to that shown for clinically healthy mice.

5. Conclusions

Thus, in the present study, we synthesized allomargaritarine (2b) directly from tryptamine and securinine by catalysis boron trifluoride as a catalyst. During the study of the biological activity of 2b we have shown its neuroprotective effects, indicated by the agent's ability to inhibit BACE1 and prevent the pathological $A\beta_{1-42}$ aggregation. The neuroprotective potential of 2b was also confirmed in an *in vivo* series of experiments on the 5xFAD transgenic mice model. It was found that the administration of 2b (15 mg/kg for 3 weeks) attenuated cognitive impairment observed in animals by improving learning performance and spatial and episodic memory in the Morris Water maze, Y-maze, and Novel object recognition tests. Moreover, at the end of *in vivo* testing, it was shown that the injection of 2b to 5xFAD mice decreased the area of amyloid plaque and MDA levels, increased GSH brain levels, and improved functioning of the respiratory chain complexes of isolated brain mitochondria. In conclusion, the results provide insights into the multitargets profile and potential application of 2b (the synthesized conjugate of alkaloid securinine and tryptamine) as a neuroprotective agent for treating Alzheimer's disease and related pathologies.

Acknowledgments

Dr. Sergey Klochkov, head of the Laboratory of Natural Compounds at the Institute of Physiologically Active Compounds of the Russian Academy of Sciences, passed away in December 2021. He was the first to synthesize and describe allomargaritarine, a conjugate of the alkaloid securinine and tryptamine. Sergey Klochkov made an outstanding contribution to the chemistry of natural compounds and was a world-famous scientist in this field. Colleagues who worked with Dr. Klochkov remember him with gratitude and are very proud that he was their mentor and leader. The authors would like to acknowledge the Center for the Collective Use (IPAC RAS) for providing the opportunity to conduct the experiments using laboratory animals. The authors also grateful to Dr. Ustyugov A. A. for the provided animals.

Author Contributions

Conceptualization, Margarita Neganova and Sergey Klochkov; methodology, Margarita Neganova, Yulia Aleksandrova, Kirill Chaprov, Alexey Semakov; investigation, Yulia Aleksandrova, Kirill Chaprov, Dmitry Tsypyshev and Alexey Semakov; data curation, Margarita Neganova; writing-original draft preparation, Margarita Neganova, Yulia Aleksandrova., Dmitry Tsypyshev and Alexey Semakov; writing-review and editing, Margarita Neganova; visualization, Margarita Neganova, Alexey Semakov, Kirill Chaprov and Yulia Aleksandrova.; supervision, Sergey Klochkov, Margarita Neganova; project administration, Margarita Neganova All authors have read and agreed to the published version of the manuscript.

Funding

This work was carried out as part of the State Assignment of IPAC RAS FFSN-2021-0013.

Competing Interests

The authors have declared that no competing interests exist.

References

1. Scheltens P, De Strooper B, Kivipelto M, Holstege H, Chételat G, Teunissen CE, et al. Alzheimer's disease. Lancet. 2021; 397: 1577-1590.
2. Mahaman YA, Embaye KS, Huang F, Li L, Zhu F, Wang JZ, et al. Biomarkers used in Alzheimer's disease diagnosis, treatment, and prevention. Ageing Res Rev. 2022; 74: 101544.
3. Lei P, Ayton S, Bush AI. The essential elements of Alzheimer's disease. J Biol Chem. 2021; 296: 100105.
4. Misrani A, Tabassum S, Yang L. Mitochondrial dysfunction and oxidative stress in Alzheimer's disease. Front Aging Neurosci. 2021; 13. doi: 10.3389/fnagi.2021.617588.
5. Sharma C, Kim SR. Linking oxidative stress and proteinopathy in Alzheimer's disease. Antioxidants. 2021; 10: 1231.
6. Chirkin E, Atkatlian W, Porée FH. The securinega alkaloids. Alkaloids Chem Biol. 2015; 74: 1-120.
7. Raj D, Łuczkiewicz M. Securinega suffruticosa. Fitoterapia. 2008; 79: 419-427.
8. Klochkov S, Neganova M. Unique indolizidine alkaloid securinine is a promising scaffold for the development of neuroprotective and antitumor drugs. RSC Adv. 2021; 11: 19185-19195.
9. Arbain D, Birkbeck AA, Byrne LT, Sargent MV, Skelton BW, White AH. The alkaloids of margaritaria indica. II, the structures of 4-epiphyllanthine, margaritarine and the structural revision of securinol A. In: Journal of the Chemical Society. Perkin transactions. I. Cambridge, UK: Royal Society of Chemistry, Cambridge; 1991. pp. 1863-1869.
10. Klochkov SG, Afanas'eva SV, Grigor'ev VV. Synthesis and biological activity of amination products of the alkaloid securinine. Chem Nat Compd. 2008; 44: 197-202.
11. Neganova ME, Klochkov SG, Afanasieva SV, Serkova TP, Chudinova ES, Bachurin SO, et al. Neuroprotective effects of the securinine-analogues: Identification of allomargaritarine as a lead compound. CNS Neurol Disord Drug Targets. 2016; 15: 102-107.

12. Neganova ME, Blik VA, Klochkov SG, Chepurnova NE, Shevtsova EF. Investigation of the antioxidant characteristics of a new tryptamine derivative of securinine and its influence on seizure activity in the brain in experimental epilepsy. Neurochem J. 2011; 5: 208-214.
13. Neganova ME, Klochkov SG, Afanasieva SV, Chudinova ES, Serkova TP, Shevtsova EF. Allomargaritarine as a basis for the creation of mitochondrial targeted potential neuroprotectors. Eur Neuropsychopharmacol. 2014; 24: S261.
14. Neganova ME, Klochkov SG, Petrova LN, Shevtsova EF, Afanasieva SV, Chudinova ES, et al. Securinine derivatives as potential anti-amyloid therapeutic approach. CNS Neurol Disord Drug Targets. 2017; 16: 351-355.
15. Phan HT, Samarat K, Takamura Y, Azo Oussou AF, Nakazono Y, Vestergaard MD. Polyphenols modulate Alzheimer's amyloid beta aggregation in a structure-dependent manner. Nutrients. 2019; 11: 756.
16. Schrödinger LLC. Schrödinger Release 2023-1: Induced Fit Docking protocol. New York, NY, US: Schrödinger, LLC; 2023.
17. Schrödinger LLC. Schrödinger Release 2023-1: Glide. New York, NY, US: Schrödinger, LLC; 2023.
18. Schrödinger LLC. Schrödinger Release 2023-1: Prime. New York, NY, US: Schrödinger, LLC; 2023.
19. Jacobson MP, Pincus DL, Rapp CS, Day TJ, Honig B, Shaw DE, et al. A hierarchical approach to all-atom protein loop prediction. Proteins. 2004; 55: 351-367.
20. Jacobson MP, Friesner RA, Xiang Z, Honig B. On the role of the crystal environment in determining protein side-chain conformations. J Mol Biol. 2002; 320: 597-608.
21. Madhavi Sastry G, Adzhigirey M, Day T, Annabhimoju R, Sherman W. Protein and ligand preparation: Parameters, protocols, and influence on virtual screening enrichments. J Comput Aided Mol Des. 2013; 27: 221-234.
22. Harder E, Damm W, Maple J, Wu C, Reboul M, Xiang JY, et al. OPLS3: A force field providing broad coverage of drug-like small molecules and proteins. J Chem Theory Comput. 2016; 12: 281-296.
23. Farid R, Day T, Friesner RA, Pearlstein RA. New insights about HERG blockade obtained from protein modeling, potential energy mapping, and docking studies. Bioorg Med Chem. 2006; 14: 3160-3173.
24. Sherman W, Day T, Jacobson MP, Friesner RA, Farid R. Novel procedure for modeling ligand/receptor induced fit effects. J Med Chem. 2006; 49: 534-553.
25. Sherman W, Beard HS, Farid R. Use of an induced fit receptor structure in virtual screening. Chem Biol Drug Des. 2006; 67: 83-84.
26. Schrödinger LLC. Schrödinger Release 2023-1: Maestro. New York, NY, US: Schrödinger, LLC; 2023.
27. Zhao Z, Fan L, Fortress AM, Boulware MI, Frick KM. Hippocampal histone acetylation regulates object recognition and the estradiol-induced enhancement of object recognition. J Neurosci. 2012; 32: 2344-2351.
28. Terunuma M, Revilla Sanchez R, Quadros IM, Deng Q, Deeb TZ, Lumb M, et al. Postsynaptic GABAB receptor activity regulates excitatory neuronal architecture and spatial memory. J Neurosci. 2014; 34: 804-816.
29. Walrave L, Vinken M, Albertini G, De Bundel D, Leybaert L, Smolders IJ. Inhibition of connexin43 hemichannels impairs spatial short-term memory without affecting spatial working memory. Front Cell Neurosci. 2016; 10: 288.

30. Arque G, Fotaki V, Fernandez D, de Lagrán MM, Arbones ML, Dierssen M. Impaired spatial learning strategies and novel object recognition in mice haploinsufficient for the dual specificity tyrosine-regulated kinase-1A (Dyrk1A). PLoS One. 2008; 3: e2575.
31. Neganova M, Aleksandrova Y, Suslov E, Mozhaitsev E, Munkuev A, Tsypyshev D, et al. Novel multitarget hydroxamic acids with a natural origin CAP group against Alzheimer's disease: Synthesis, docking and biological evaluation. Pharmaceutics. 2021; 13: 1893.
32. Aleksandrova Y, Chaprov K, Podturkina A, Ardashov O, Yandulova E, Volcho K, et al. Monoterpenoid epoxidiol ameliorates the pathological phenotypes of the rotenone-induced Parkinson's disease model by alleviating mitochondrial dysfunction. Int J Mol Sci. 2023; 24: 5842.
33. Connor Robson N, Peters OM, Millership S, Ninkina N, Buchman VL. Combinational losses of synucleins reveal their differential requirements for compensating age-dependent alterations in motor behavior and dopamine metabolism. Neurobiol Aging. 2016; 46: 107-112.
34. Ninkina N, Papachroni K, Robertson DC, Schmidt O, Delaney L, O'Neill F, et al. Neurons expressing the highest levels of γ-synuclein are unaffected by targeted inactivation of the gene. Mol Cell Biol. 2003; 23: 8233-8245.
35. Stokes G. An improved Congo red method for amyloid. Med Lab Sci. 1976; 33: 79-80.
36. Doughty MJ. A grid-based nucleus counting method for estimates of the density of superficial conjunctival cells from impression cytology samples taken from normal healthy human eyes. Curr Eye Res. 2017; 42: 1228-1234.
37. Bansode SB, Jana AK, Batkulwar KB, Warkad SD, Joshi RS, Sengupta N, et al. Molecular investigations of protriptyline as a multi-target directed ligand in Alzheimer's disease. PLoS One. 2014; 9: e105196.
38. Rostagno A, Calero M, Holton JL, Revesz T, Lashley T, Ghiso J. Association of clusterin with the BRI2-derived amyloid molecules ABri and ADan. Neurobiol Dis. 2021; 158: 105452.
39. Wolfer DP, Madani R, Valenti P, Lipp HP. Extended analysis of path data from mutant mice using the public domain software Wintrack. Physiol Behav. 2001; 73: 745-753.
40. Alzheimer's Disease International. The global voice on dementia [Internet]. London, UK: Alzheimer's Disease International; 2023. Available from: https://www.alzint.org/.
41. Rostagno AA. Pathogenesis of Alzheimer's disease. Int J Mol Sci. 2022; 24: 107.
42. Jaroudi W, Garami J, Garrido S, Hornberger M, Keri S, Moustafa AA. Factors underlying cognitive decline in old age and Alzheimer's disease: The role of the hippocampus. Rev Neurosci. 2017; 28: 705-714.
43. Chen X, Sun G, Tian E, Zhang M, Davtyan H, Beach TG, et al. Modeling sporadic Alzheimer's disease in human brain organoids under serum exposure. Adv Sci. 2021; 8: 2101462.
44. Gupta SP, Patil VM. Recent studies on design and development of drugs against Alzheimer's disease (AD) based on inhibition of BACE-1 and other AD-causative agents. Curr Top Med Chem. 2020; 20: 1195-1213.
45. Lichtenthaler SF, Tschirner SK, Steiner H. Secretases in Alzheimer's disease: Novel insights into proteolysis of APP and TREM2. Curr Opin Neurobiol. 2022; 72: 101-110.
46. Prati F, Bottegoni G, Bolognesi ML, Cavalli A. BACE-1 inhibitors: From recent single-target molecules to multitarget compounds for Alzheimer's disease: Miniperspective. J Med Chem. 2018; 61: 619-637.

47. Li QS, Francke S, Snoeys J, Thipphawong J, Romano G, Novak GP. Genome-wide association study of abnormal elevation of ALT in patients exposed to atabecestat. BMC Genomics. 2023; 24: 513.
48. Sims JR, Selzler KJ, Downing AM, Willis BA, Aluise CD, Zimmer J, et al. Development review of the BACE1 inhibitor lanabecestat (AZD3293/LY3314814). J Prev Alzheimers Dis. 2017; 4: 247-254.
49. Namioka S, Yoshida N, Konno H, Makabe K. Residue-specific binding mechanisms of thioflavin T to a surface of flat β-sheets within a peptide self-assembly mimic. Biochemistry. 2020; 59: 2782-2787.
50. Oakley H, Cole SL, Logan S, Maus E, Shao P, Craft J, et al. Intraneuronal β-amyloid aggregates, neurodegeneration, and neuron loss in transgenic mice with five familial Alzheimer's disease mutations: Potential factors in amyloid plaque formation. J Neurosci. 2006; 26: 10129-10140.
51. Hoang TH, Ho DV, Van Phan K, Le QV, Raal A, Nguyen HT. Effects of Hippeastrum reticulatum on memory, spatial learning and object recognition in a scopolamine-induced animal model of Alzheimer's disease. Pharm Biol. 2020; 58: 1107-1113.
52. Binyamin O, Nitzan K, Frid K, Ungar Y, Rosenmann H, Gabizon R. Brain targeting of 9c, 11t-conjugated linoleic acid, a natural calpain inhibitor, preserves memory and reduces Aβ and P25 accumulation in 5XFAD mice. Sci Rep. 2019; 9: 18437.
53. Kraeuter AK, Guest PC, Sarnyai Z. The Y-maze for assessment of spatial working and reference memory in mice. In: Pre-clinical models: Techniques and protocols. New York, NY, US: Humana Press; 2019. pp. 105-111.
54. McAlpine CS, Park J, Griciuc A, Kim E, Choi SH, Iwamoto Y, et al. Astrocytic interleukin-3 programs microglia and limits Alzheimer's disease. Nature. 2021; 595: 701-706.
55. Okamoto M, Gray JD, Larson CS, Kazim SF, Soya H, McEwen BS, et al. Riluzole reduces amyloid beta pathology, improves memory, and restores gene expression changes in a transgenic mouse model of early-onset Alzheimer's disease. Transl Psychiatry. 2018; 8: 153.
56. Nunez J. Morris water maze experiment. J Vis Exp. 2008; e897. doi: 10.3791/897.
57. Fjell AM, McEvoy L, Holland D, Dale AM, Walhovd KB, Alzheimer's Disease Neuroimaging Initiative. What is normal in normal aging? Effects of aging, amyloid and Alzheimer's disease on the cerebral cortex and the hippocampus. Prog Neurobiol. 2014; 117: 20-40.
58. Katabathula S, Wang Q, Xu R. Predict Alzheimer's disease using hippocampus MRI data: A lightweight 3D deep convolutional network model with visual and global shape representations. Alzheimers Res Ther. 2021; 13: 104.
59. Wirths O, Walter S, Kraus I, Klafki HW, Stazi M, Oberstein TJ, et al. N-truncated $A\beta_{4-x}$ peptides in sporadic Alzheimer's disease cases and transgenic Alzheimer mouse models. Alzheimers Res Ther. 2017; 9: 80.